Optical transitions in semiconducting zigzag carbon nanotubes with small diameters: A first-principles broad-range study

Saloome Motavas, Andre Ivanov, and Alireza Nojeh*
Department of Electrical and Computer Engineering, The University of British Columbia, Vancouver, British Columbia, Canada V6T 1Z4
(Received 26 February 2010; revised manuscript received 27 May 2010; published 26 August 2010)

We study all possible band-to-band transitions between 12 valence and 16 conduction bands of (8,0), (10,0), and (7,0) nanotubes and calculate the corresponding dipole moments using first-principles methods in a wide ultraviolet-visible-infrared range of photon energies. The goal is to investigate the optical transitions and the selection rules for nanotubes with small diameters in a broad range of energies, taking into account the curvature and rehybridization effects on the dipole moment. Our calculations show the conservation of a modified quantum number, $\hat{m}$, for all the transitions and reversal of the horizontal parity. Besides the π-π^* transitions, we observe the possibility of π-σ^*, σ-π^*, and σ-σ^* transitions. In fact, the maximum dipole moment for the three nanotubes corresponds to the transition between valence and conduction bands that are both of σ nature. The maximum transition rate for an (8,0) nanotube happens at approximately 1.42 eV, corresponding to the transition between the first valence and fourth conduction bands and mapping to the infrared region. The maximum of transition rate for (10,0) and (7,0) nanotubes happens at 0.79 eV and 3.03 eV, respectively. There exist high absorption probabilities in the infrared and visible region in all three nanotubes. Also, high absorption probability in the low ultraviolet region is demonstrated, mostly as a result of σ-σ^* transitions.

DOI: 10.1103/PhysRevB.82.085442 PACS number(s): 78.67.Ch, 78.40.Ri, 73.22.−f

I. INTRODUCTION

Carbon nanotubes (CNTs) are nanoscale materials that are well known for their unique properties arising from their one-dimensional nature and strong carbon-carbon bond in their structure. One of their attractive areas of application is nanophotonics. Semiconducting nanotubes are direct band-gap materials and their optical absorption and emission properties have been studied both theoretically and experimentally. The unique optical behavior of these structures stems from their one-dimensionality and sharp van Hove singularities (VHS) in their density of states. Photoluminescence from individual single-walled nanotubes (SWNTs) has been observed[1–3] and the photoconductivity of these structures has been studied.[4,5] Various research groups have experimentally measured the optical absorption spectra of CNTs and explored the structural dependence of these spectra.[6–10] The optical spectra and their dependence on the diameter and chirality have also been investigated theoretically.[11–16] The optical spectra of SWNTs in the visible-infrared region have been studied using first-principles methods and the effect of excitons on the absorption spectra has been explored.[11–13] A quantitative analysis of the optical spectra in the ultraviolet-visible-infrared region based on tight-binding (TB) band-structure calculations has been reported.[14] Ultraviolet optical absorption in CNTs has also been recently studied with first-principles methods.[15,16] In this paper, we study the optical transition mechanisms for (8,0), (10,0), and (7,0) nanotubes which are semiconducting zigzag CNTs with subnanometer diameters of ~0.63 nm, ~0.78 nm, and ~0.55 nm, respectively, in the broad range of ultraviolet-visible-infrared. The goal is to take into account the possible effects of curvature and rehybridization on the optical transitions, selection rules, and dipole moments, as well as attribute the spectral peaks to the relevant transitions. Optical transition energies in nanotubes have been previously calculated with extended TB (ETB) and first-principles methods, showing good agreement with experimental results.[11,17] However, to our knowledge, transition dipole moments and selection rules for nanotubes have not been investigated by any method other than the π-orbital TB approach.[18–22] Here, we calculate the dipole moment for each of the transitions based on first-principles approaches and the density-functional theory (DFT). These methods are computationally expensive compared to the TB approximation. However, they can provide more accurate molecular orbitals and band structures, which can result in a more realistic estimate of the transition dipole moment, especially for CNTs with small diameters.

The transition dipole moment is a vector quantity associated with the transition of electrons between two states with the magnitude of the dipole indicating the probability of this transition. The dipole moment is not only needed for calculating the transition rates and absorption spectra but also provides valuable insight into interband transition mechanisms and selection rules. Transition dipole moments for nanotubes have so far been reported only based on the π-orbital TB/zone-folding approach. (From here on, unless otherwise specified, by TB we mean to refer to the π-orbital TB method within the zone-folding approach.) This method offers a highly valuable intuitive interpretation of the electronic structure and is useful for the qualitative description of the transition rates and absorption properties. However, the simplifications used in this method impose limitations and may result in significant inaccuracies. For example, π-orbital TB does not treat the σ-π hybridization resulting from the curvature of the nanotube sidewall, which is pronounced especially in SWNTs with diameters smaller than 1 nm.[23] It has been shown that it fails in accurately predicting the conduction bands in particular.[24] Also, since only π orbitals are included in this approximation, the possibility of other tran-

sitions that may occur in CNTs is neglected.[25,26] Finally, TB does not include many-body exchange and correlation effects.

One can calculate the interband transition rates using the perturbation theory and Fermi's golden rule. According to the golden rule, the transition rate, W_{if}, between an initial state, ψ_i, and a final state, ψ_f, can be calculated from the following:

$$W_{if} = \frac{2\pi}{\hbar}|H'_{if}|^2\rho_f, \tag{1}$$

where $\hbar$ is the reduced Planck constant, ρ_f is the density of states around the final state, and H'_{if} is the absorption matrix element. In our case H'_{if} is the optical perturbation Hamiltonian matrix element given by

$$H'_{if} = i\frac{e\hbar}{m\omega}\sqrt{\frac{I}{\epsilon c}}e^{i(\omega_f-\omega_i-\omega)t}P\cdot D, \tag{2}$$

where I, ω, and P are the intensity, angular frequency, and polarization vector of the incident light, respectively, and i and f refer to the initial and final states. Electron mass and the elementary charge are represented by m and e, respectively. c is the speed of light and ϵ is the dielectric constant. D is the electric dipole vector given by

$$D = \langle\Psi_f|\nabla|\Psi_i\rangle. \tag{3}$$

Absorption of light polarized perpendicular to the nanotube axis is known to be suppressed compared to that of parallel-polarized light.[27] Therefore, here we focused on the z-polarized light with the nanotube lying along the z direction.

II. METHODOLOGY AND RESULTS

(8,0), (10,0), and (7,0) SWNTs were relaxed by geometry optimization in the software package GAUSSIAN 03.[28] The diameters of these nanotubes are less than 1 nm in all three cases and we expect curvature-induced effects to be pronounced in them. In order to mimic an infinitely long nanotube, one unit cell of the nanotube with periodic boundary conditions was used. The orbital energies and wave functions were then obtained using both GAUSSIAN 03 and GAUSSIAN 09 (Ref. 29) with various levels of theory and basis sets. Here, we discuss the results obtained from DFT calculations using Becke-Lee-Yang-Parr (BLYP) (Refs. 30 and 31) and Becke3-Lee-Yang-Parr (B3LYP) (Refs. 30–32) exchange-correlation potentials, as well as those obtained from the restricted Hartree-Fock (RHF) method, using 6–31G basis sets. The discussions are mainly based on BLYP calculations for an (8,0) nanotube. The rest of the results are presented for comparison purposes.

To calculate the dipole moment according to Eq. (3), the wave function for each valence and conduction band was extracted from the simulations. The derivative of the wave function for the studied valence band was calculated using the method of finite differences and the integral was performed. Approximately, 2×10^7 grid points with a spacing of 0.044 Å in all directions were used for calculations in the three-dimensional space. The number of grid points in the x and y directions varied based on the diameter of the nanotube. As an example, a $300\times300\times221$ grid was used to discretize the molecular orbitals for the BLYP calculations in an (8,0) nanotube. Further refining of the grid did not lead to any significant change in the results. Gaussian gives the wave functions only at the Γ point ($k_z=0$). Therefore, dipole moments were calculated only at this k point, which in the case of zigzag nanotubes turns out to be where the VHS occur. Since the density of states is mainly due to these singularities, the dipole moment at the Γ point is expected to have the most significant effect on the overall rate of transition to a specific subband. The dipole moment was calculated for transitions between all the possible combinations of valence and conduction bands for 12 valence and 16 conduction bands. As an example, Fig. 1(b) shows the squared magnitude of the dipole for transitions between the highest occupied molecular orbital (HOMO) and all the first 16 conduction bands of an (8,0) nanotube. Figure 1(a) depicts the calculated band structure with the BLYP method.

As we can see from Fig. 1(a), in contrast with TB results, the band structure resulting from the first-principles calculations is not symmetric with respect to the Fermi level. As depicted in Fig. 1(b), $D_z\approx0$ for all the transitions except those to the fourth (A) and sixth (B) conduction bands. The first transition, in fact, occurs between the HOMO and the fourth conduction band instead of happening across the band gap. Table I summarizes the results and analysis of an (8,0) nanotube for the first 12 valence bands. Only simulation results with squared dipole value of more than 0.005 ($\sim$0.01% of the maximum value obtained from our simulations) are shown and other transitions are not listed in the table for the sake of conciseness. The possible transitions are determined and the square value of the dipole moments (arbitrary units) and the photon energy required for each transition are shown. The selection rules have also been studied for these transitions and the symmetry parameters have been determined.

Dipole selection rules which govern light absorption and emission processes in CNTs only allow electronic transitions between specific valence and conduction bands for light polarized along the tube axis. These selection rules can be derived based on the symmetry of nanotubes and the symmetry-based quantum numbers. For achiral tubes (armchair and zigzag), the irreducible representations of the carbon nanotube symmetry groups are in the form of ${}_kX^h_m$, where k is the wave vector along the nanotube axis, m is the quasiangular momentum related to the rotational symmetry, and h is the parity with respect to the horizontal mirror plane, σ_h, denoted by "+" for even states and "−" for odd ones. X can be A or B for one-dimensional, E for two-dimensional, and G for four-dimensional representations. A and B also indicate the parity quantum number with respect to the vertical mirror plane, σ_v, where A corresponds to even and B to odd parity.

Because of its ${}_0A^-_0$ symmetry, z-polarized light preserves the angular momentum quantum number, m. However, the horizontal parity is reversed upon this interaction since

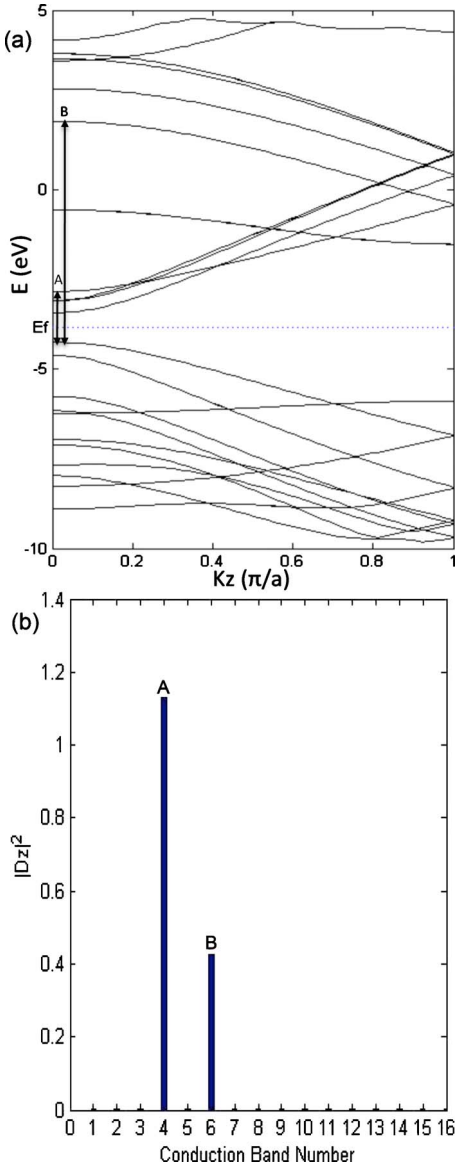

FIG. 1. (Color online) DFT (BLYP/6–31G) calculation of (a) band structure and (b) dipole moment magnitude squared (arbitrary units) for transitions between HOMO and the first 16 conduction subbands of an (8,0) nanotube, showing the allowed transitions to the (A) fourth and (B) sixth conduction subbands (a is the translational period along the tube axis).

z-polarized light carries odd σ_h and vertical parity is conserved because of even σ_v.[33]

In our studies, the type of the orbitals, their horizontal parity, and the angular momentum number, m, are determined by plotting the spatial distribution of the orbitals for each subband. Figure 2 shows example orbitals for two different subbands (c5 and v6) of the (8,0) nanotube. The out of plane (out of the nanotube surface) orbital in Fig. 2(a) indicates a π orbital while the in-plane orbital in Fig. 2(b) suggests its origin to be mainly from σ bonds. In this work, the angular momentum number, m, for each orbital corresponds to half of the number of nodes of its wave function around the circumference.

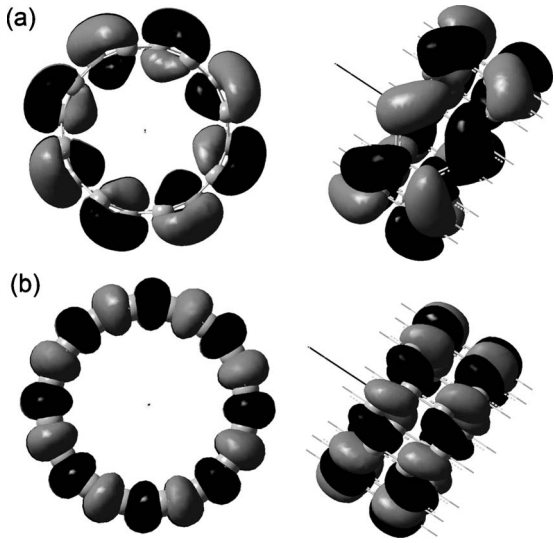

FIG. 2. Molecular orbitals for the (a) fifth conduction band and (b) sixth valence band of an (8,0) nanotube calculated with BLYP/6–31G. Left: view along the tube axis. Right: view perpendicular to the tube axis.

III. DISCUSSION AND ANALYSIS

Based on our observations, in order to explain all the allowed transitions, the angular momentum number, m, defined before, needs to be transformed to a modified angular momentum number, $\hat{m}$, according to the following:

$$\hat{m} = m + \hat{M}n, \tag{4}$$

where n is the index of the nanotube and $\hat{M}$ is an integer determined in a way that the modified quantum number satisfies the following range criteria:

$$\hat{m} \in \left(\frac{-n}{2}, \frac{n}{2}\right]. \tag{5}$$

Table I shows that this modified angular momentum number, $\hat{m}$ [which is reminiscent of the helical angular momentum, $\tilde{m}$ (Ref. 33)], is conserved for all the transitions.

From Table I, the maximum dipole moment in an (8,0) nanotube corresponds to the transition from the seventh valence band to the 15th conduction band, which is a σ-σ^* transition. In general, the calculated dipole moment for the σ-σ^* transitions have much larger values compared to the other transitions. However, since these transitions normally happen over large energy gaps, their corresponding transition rates are undermined [see Eq. (2)]. Our simulations for (10,0) and (7,0) nanotubes indicate a similar trend. The maximum dipole moment for transitions between the first 12 valence and 16 conduction bands of a (10,0) nanotube corresponds to the transition from the tenth valence band to the 14th conduction band, and it happens from the sixth valence band to the 14th conduction band for a (7,0) nanotube. Both of these transitions are of σ-σ^* nature.

Figures 3(a) and 3(b) show $|H'|^2$ and W (transition rate) at the Γ point, according to Eqs. (1) and (2), respectively, versus the required energy for the transitions in an (8,0) nano-

TABLE I. Summary of the results for an (8,0) nanotube using the BLYP/6–31G method. The allowed transitions from each valence band are determined and the dipole moment magnitude (arbitrary units) and the photon energy required for those transitions are calculated (transitions with the relative dipole moment squared of less than 0.005 are not listed in the table for brevity). The parameters related to the selection rules are listed.

Valence	$\hat{m}_v$	h	Conduction	$\hat{m}_c$	h	$\Delta\hat{m}$	Transition	Energy (eV)	$\lvert D_z\rvert^2$
v1	±3	+	c4	±3	−	0	π-π^*	1.42	1.129
			c6	±3	−	0	π-π^*	6.16	0.426
v2	±2	−	c3	±2	+	0	π-π^*	1.53	2.296
			c14	±2	+	0	π-σ^*	10.06	0.005
v3	±1	−	c2	±1	+	0	π-π^*	2.67	3.540
			c12	±1	+	0	π-σ^*	10.25	0.222
			c13	±1	+	0	π-σ^*	10.58	1.668
v4	0	−	c1	0	+	0	π-π^*	2.73	3.886
			c8	0	+	0	π-σ^*	9.75	2.224
v5	4	+	c5	4	−	0	π-π^*	5.67	0.999
v6	0	−	c11	0	+	0	σ-σ^*	11.12	9.645
v7	0	+	c7	0	−	0	σ-π^*	9.93	4.934
			c15	0	−	0	σ-σ^*	13.89	51.572
v8	±1	+	c9	±1	−	0	σ-π^*	11.31	1.935
			c16	±1	−	0	σ-σ^*	14.50	45.828
v9	±1	−	c12	±1	+	0	σ-σ^*	12.45	10.131
v10	±3	+	c4	±3	−	0	π-π^*	5.42	0.830
			c6	±3	−	0	π-π^*	10.16	0.005
v11	±2	+	c10	±2	−	0	$\pi\backslash\sigma$-π^*	12.69	0.318
v12	±2	−	c14	±2	+	0	σ-σ^*	15.52	9.736

tube. Because of the E^{-2} dependence of the transition rate (E is the transition energy), the probability of transition for the higher energy transitions, that generally correspond to the σ-σ^* transitions, is rather weak. Also, the density of states (DOS) has a significant effect on the strength of transitions. For example, although the second transition has a much higher dipole moment compared to the first one, its probability of transition is less than the first transition because of its lower DOS. The maximum of absorption happens for the first transition at around 1.42 eV, corresponding to the transition between the first valence and fourth conduction bands and mapping to the infrared region. There is also a high probability of absorption for 1.53 eV (infrared), and 2.67 and 2.73 eV (blue) lights. Interestingly, there is also a relatively high absorption probability at around 12.45, 13.89, and 14.50 eV, mapping approximately to the low ultraviolet (12.4–14.1 eV) range.

The first seven peaks in the absorption spectra are related to π-π^* transitions, which cover the infrared, visible and also the near UV region. As shown in Table I, transitions from a valence band to several conduction bands are possible. In fact, in some cases a transition from a valence π band happens to more than one conduction π band, in contrast with what is presumed in the TB approximation. For example, as shown in Fig. 1(b), transitions from HOMO can be made to either the fourth or the sixth conduction bands.

Table I also reveals that optical transitions are not limited to π-π^* transitions only; π-σ^*, σ-π^*, and σ-σ^* transitions are also allowed and can happen with a relatively high probability in some cases. For example, the three strongest peaks in the low UV region at 12.45, 13.89, and 14.50 eV (Fig. 3) are all related to the σ-σ^* transitions. These transitions can provide insight into the possibility of optical absorption in the high-frequency regions and the ultraviolet applications of carbon nanotubes.

The first two peaks in our calculations closely follow the experimental data in Ref. 7. Table II compares the first and second optical transition energies and their ratio obtained from different methods. The energies obtained from BLYP calculations are closer to the experimental values compared to the B3LYP and RHF results. The E_{22}/E_{11} ratio from BLYP results is equal to 1.08, close to the value of 1.09 from the local-density-approximation (LDA) calculations in Ref. 11 and in significantly better agreement with the experimental

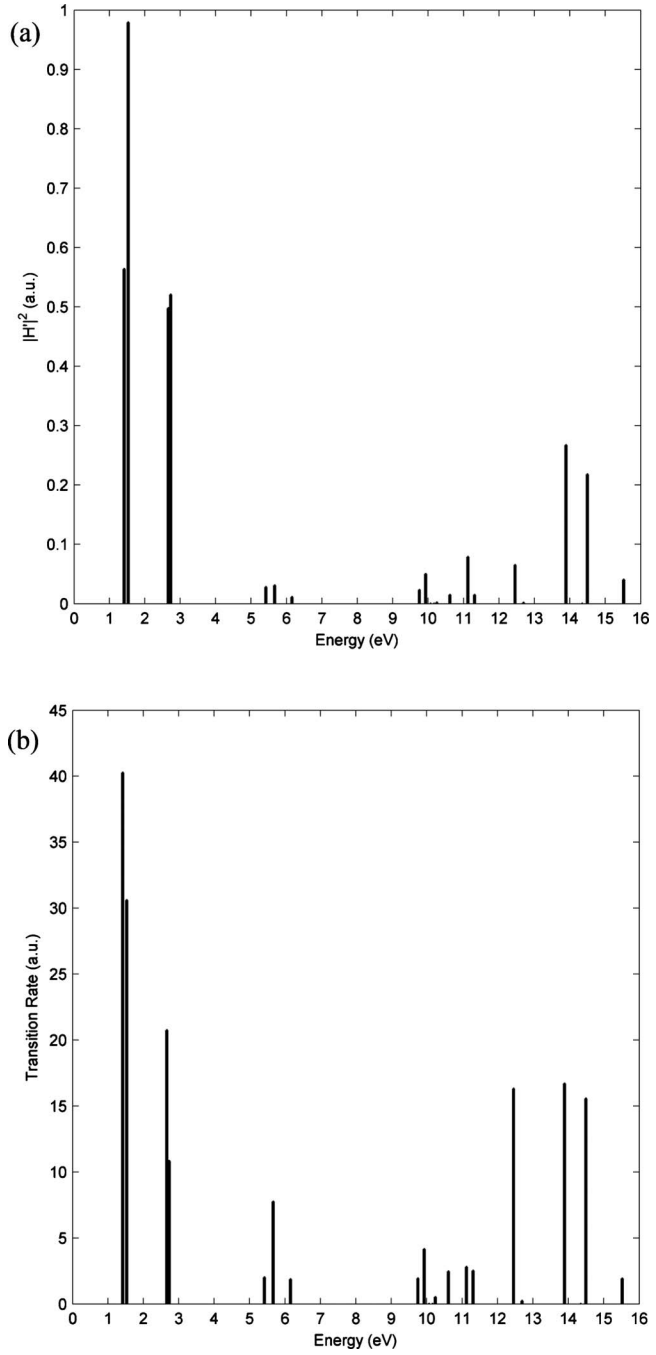

FIG. 3. (a) $|H'|^2$ and (b) W (transition rate) at the Γ point versus the energy of transition for an (8,0) nanotube, showing the maximum absorption at 1.42 eV (infrared) and relatively high absorption probability in the visible and ultraviolet regions.

results of 1.17 reported in Ref. 7 than the value of ~1.6 predicted by an improved TB model including third-order neighbors.[6,34] We also see that the extended tight-binding model, which takes into account the σ bands and the curvature effects, provides a much better agreement to the experimental values compared to the π-orbital TB.[17] However, calculation of the dipole moment and study of the selection rules for nanotubes have not been done beyond the π-orbital TB.

TABLE II. Lowest two optical transition energies and their ratio for an (8,0) nanotube.

	E_{11} (eV)	E_{22} (eV)	E_{22}/E_{11}
BLYP	1.42	1.53	1.08
B3LYP	2.12	2.26	1.07
RHF	5.00	5.17	1.03
LDA[a]	1.39	1.51	1.09
GW[a]	2.54	2.66	1.05
BS[a]	1.55	1.80	1.16
TB[b]			1.60
ETB[c]	1.30	1.62	1.25
Experiment[d]	1.60	1.88	1.17

[a]LDA, GW approximation, and BS equation, Ref. 11.
[b]Improved tight-binding, Refs. 6 and 34.
[c]Extended tight-binding, calculated according to Ref. 17.
[d]References 6 and 7.

As noted in Refs. 11 and 12 and shown in Table II [Bethe-Salpeter (BS) results], excitonic effects that are ignored in our calculations can qualitatively affect the optical absorption results. This may explain the ~8% discrepancy between our results and the experimental data. It has been shown that the quasiparticle corrections and electron-hole interactions affect the band gap and play a crucial role in the optical absorption spectra of semiconducting carbon nanotubes.[11,12]

Figures 4(a) and 4(b) show the transition rate at the Γ point versus the transition energy for (10,0) and (7,0) nanotubes, respectively. The maximum of absorption for (10,0) and (7,0) nanotubes happens at 0.79 eV and 3.03 eV, respectively. Comparing the transition plots for the three nanotubes shows a few similarities in their absorption spectra. The majority of transitions with high probability happen in the infrared and visible range for the three nanotubes. Except in the range of ~5–6 eV, no probability of transition is observed beyond the visible range up to 9 eV. However, considerable transition probabilities exist in the low UV range, mostly as a result of σ-σ^* transitions. While the maximum absorption probability happens at the first transition and maps to the infrared region for (8,0) and (10,0) nanotubes, the maximum transition rate for a (7,0) nanotube happens at 3.03 eV (violet) and with a significantly higher relative probability compared to the maximum for the other two nanotubes. The reason for this high probability of transition can be attributed to the nearly dispersionless band at the fourth conduction band in the band structure of the (7,0) nanotube, which results in a very high DOS and therefore high transition rate.

Optical spectroscopy measurements carried out on SWNTs have shown strong peaks in the infrared and visible ranges and revealed the dependence of these peaks on the diameter and chirality of the nanotubes.[6–9] The possibility of fluorescence and infrared photoluminescence for isolated SWNTs in aqueous suspensions or suspended SWNTs in air have also been reported.[1,3] Photoconductivity experiments on SWNTs have also shown peaks in the infrared and visible ranges.[4,5]

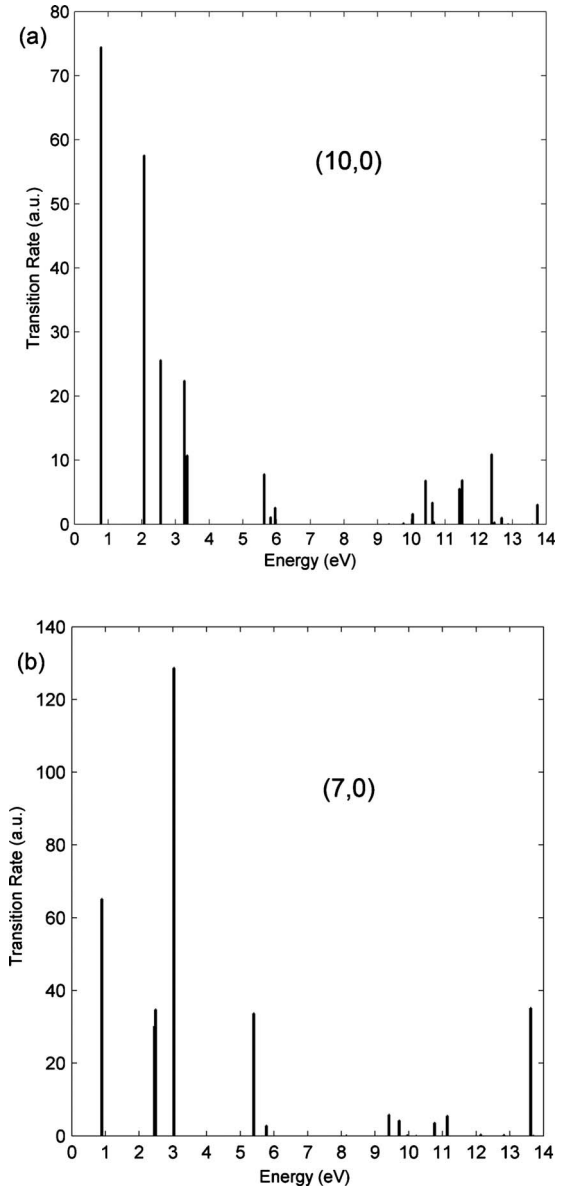

FIG. 4. Transition rate at the Γ point versus the energy of transition for (a) (10,0) and (b) (7,0) nanotubes, showing high probability of transitions in the infrared, visible and low UV regions. Maximum of absorption for (10,0) and (7,0) nanotubes is located at 0.79 eV and 3.03 eV, respectively.

Ultraviolet spectroscopy has revealed the dependence of the spectrum on the nanotube diameter.[35] UV absorption components in the optical spectra of carbon nanotubes have usually been attributed to the π-plasmon excitations.[36] π-π^* transitions at the X ($K=\frac{\pi}{a}$) point of the band structure have also been suggested to be responsible for UV absorption.[15] Our results show that π-σ^*, σ-π^*, and σ-σ^* transitions can also contribute to the UV components of the spectra.

IV. COMPARISON WITH TIGHT BINDING

To understand the discrepancies between our dipole moment results and the ones obtained from the π-orbital TB model (within the zone-folding scheme), we first compare our calculated band structure with the TB band structure (Figs. 5 and 6). In TB, the valence and conduction bands are symmetric with respect to the Fermi level as shown in Figs. 5(a) and 6(a), and every corresponding valence and conduction bands have the same angular momentum quantum number and opposite horizontal parity. Therefore, transitions between each pair of conduction and valence bands of a zigzag nanotube satisfy the selection rules. In reality, however, the π bands are not the only bands contributing to the electronic dispersion relation of nanotubes. Especially for nanotubes with a small diameter, the σ-π hybridization alters the band structure and electronic characteristics significantly.

Our band-structure results are consistent with other existing first-principles calculations of the band structure such as those reported in Ref. 24. Valence bands from TB compare relatively well with the π bands from the DFT calculations, especially for the first few bands with higher energies. Bands resulting from σ bonds or strong π-σ hybridization are shown with dashed lines in Fig. 5(b). The discrepancy between the two band structures is more apparent for the conduction bands. As shown in Fig. 6(b), the conduction bands are shifted down, distorted, and have switched places and, overall, they cease to form a symmetric image of the valence bands, consistent with calculations in Ref. 24. This could be partially due to curvature and rehybridization effects. Such a strong down-bending effect has also been confirmed experimentally.[1,2] As the diameter of the nanotube increases, these effects become less noticeable and the π band structure approaches the one predicted in TB. However, for small-diameter tubes, the discrepancies in the electronic band structures calculated from the first-principles methods and the TB approximation are at the core of the inconsistencies between the resulting optical transition dipole moments.

Figure 7 compares the dipole moment at the Γ point between the valence and conduction π-subbands with the same index, resulting from our calculations using both TB and DFT (BLYP/6–31G) electronic structures. A similar trend is observed for the three nanotubes. The dipole moment square for each nanotube is normalized based on the TB value for the last subband and the subband indices are assigned in a manner consistent with the TB subband number assignment. Even for these subbands, although there is general agreement between TB and DFT results, there are clear and significant differences. Moreover, in contrast with the TB prediction, the dipole moment calculated using DFT does not show a monotonic increase with the subband number.

Neglecting the curvature effects can also affect the density of states and consequently the calculated probability of transition. For example, according to the TB calculations in Ref. 20 for $(n,0)$ zigzag nanotubes with n even, there is a sharp peak in the absorption spectrum corresponding to the transition to the conduction subband with $m=\frac{n}{2}$. This maps to the transition with the energy of 5.67 eV in Fig. 3(b) which does not indicate a very strong peak. The reason for the strong peak in the TB calculations is the dispersionless band for $m=\frac{n}{2}$, which results in a high DOS. Our band-structure calculations for (8,0) and (10,0) nanotubes, however, show that this band is not completely dispersionless and its associated DOS is not as high as what is predicted by TB. On the other

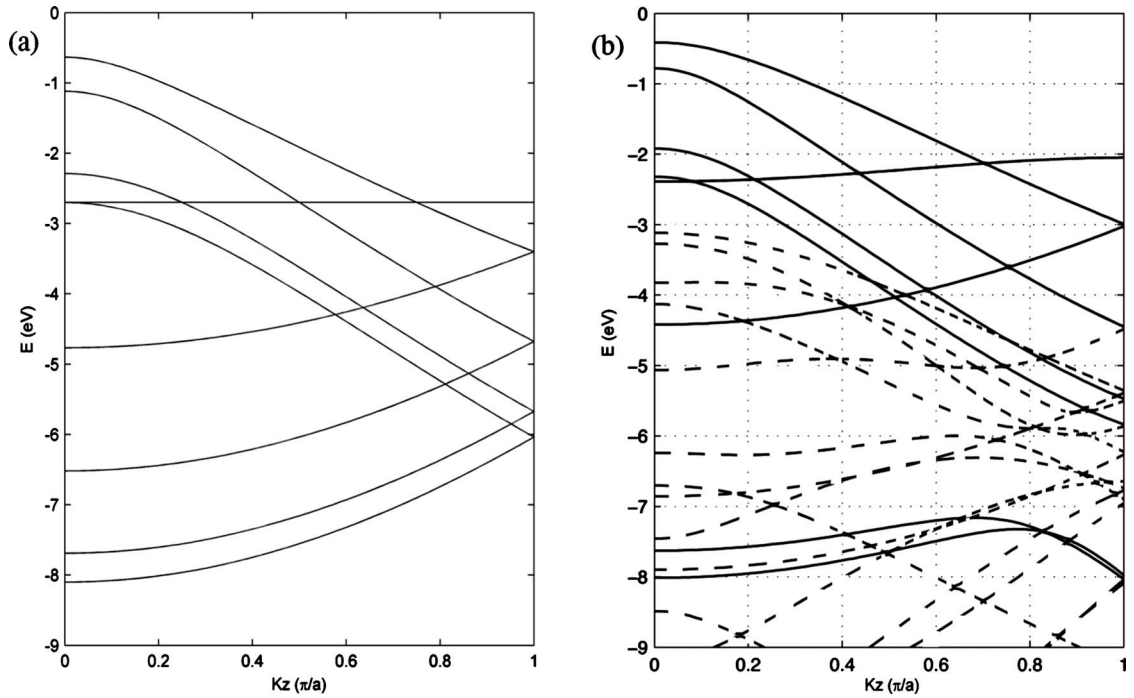

FIG. 5. Valence bands of an (8,0) nanotube with (a) the π-band TB method (plotted using the formulas in Ref. 37) and (b) DFT (BLYP/6–31G) calculations. The dashed lines indicate bands resulting from the σ or strongly hybridized π-σ orbitals. The solid lines correspond to the π orbitals and resemble the TB bands. The Fermi level is located at zero.

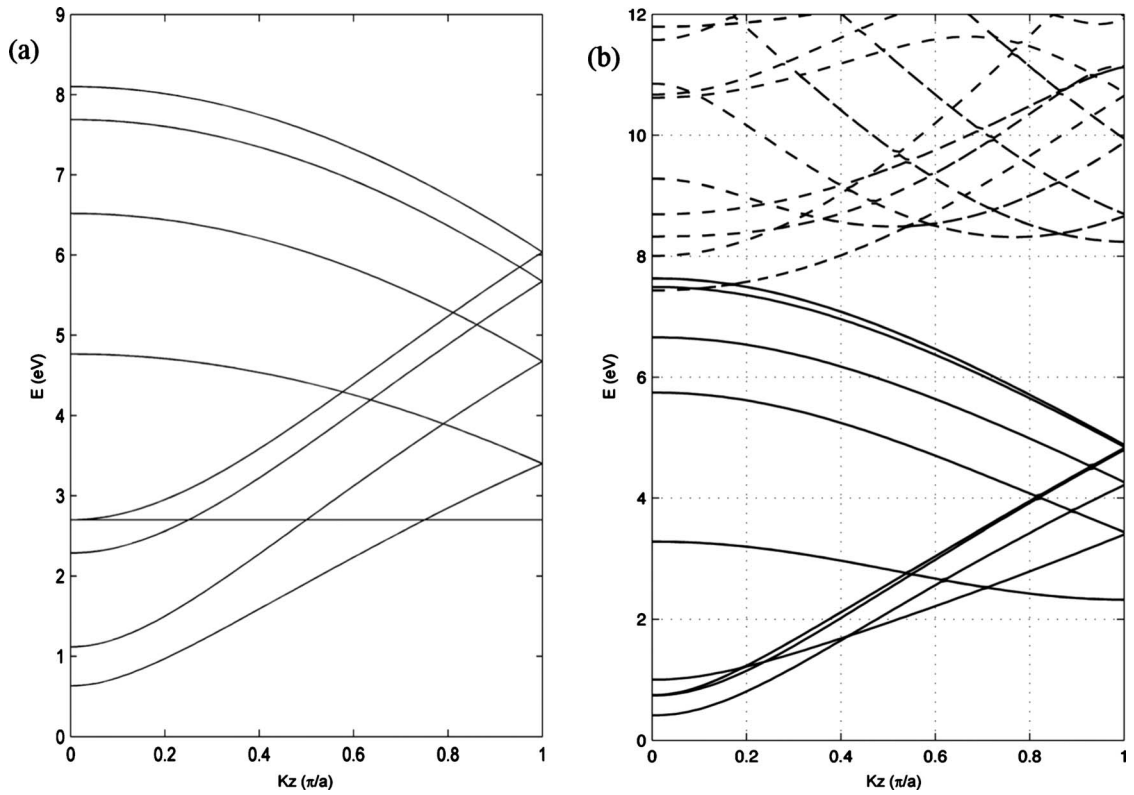

FIG. 6. Conduction bands of an (8,0) nanotube with (a) the π-band TB method (plotted using the formulas in Ref. 37) and (b) DFT (BLYP/6–31G) calculations. Conduction bands in the DFT calculations are shifted down and have switched place (see the four lowest bands near $k_z=0$) compared to the TB bands. The dashed lines indicate bands resulting from the σ orbitals. The solid lines correspond to the π orbitals. The Fermi level is located at zero.

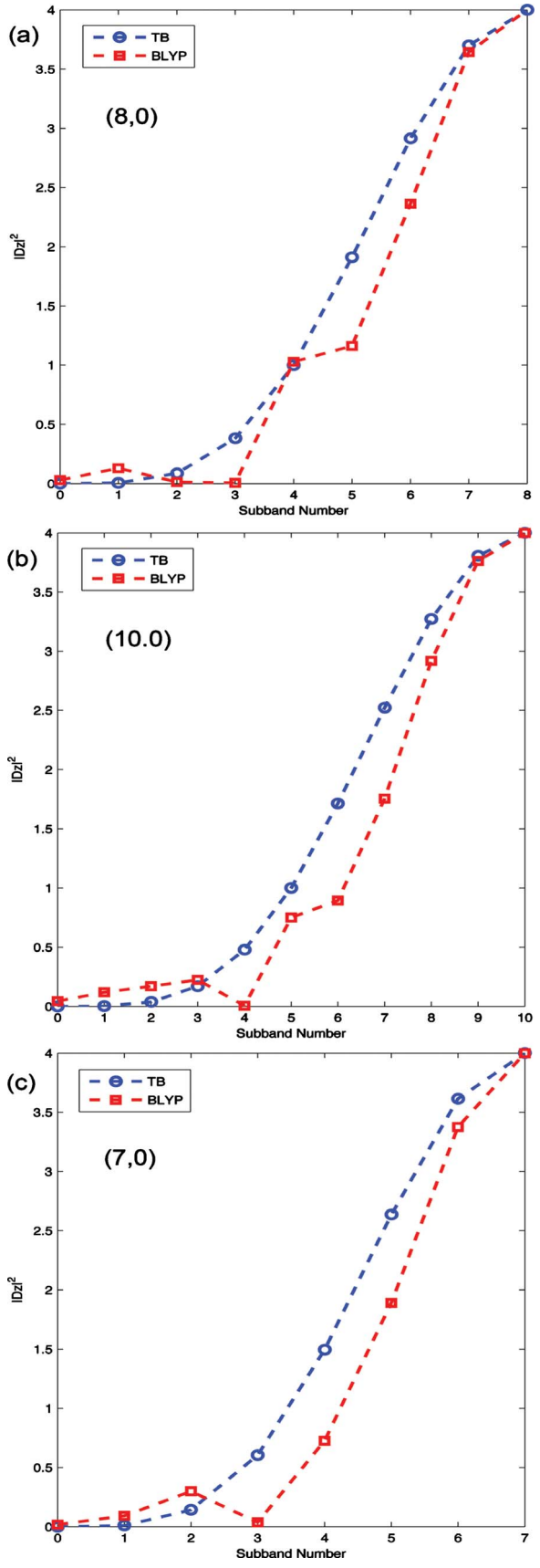

FIG. 7. (Color online) Magnitude squared of the dipole moment for (a) (8,0), (b) (10,0), and (c) (7,0) nanotubes at the Γ point with the TB and DFT (BLYP/6–31G) methods.

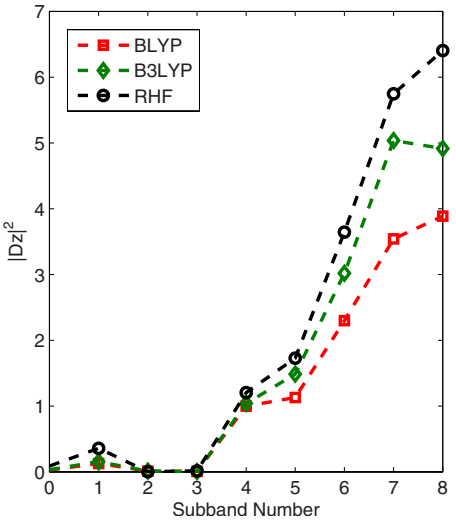

FIG. 8. (Color online) Magnitude squared of the dipole moment for an (8,0) nanotube at the Γ point with the DFT (BLYP/6–31G and B3LYP/6–31G) and RHF/6–31G methods.

hand, our band-structure calculations for the (7,0) nanotube result in a nearly dispersionless band near the Γ point at the $m=\frac{n-1}{2}$ subband, which is not dispersionless according to the TB calculations. This conduction band in fact leads to the maximum of absorption probability and a sharp peak in the optical spectrum of the (7,0) nanotube because of its high DOS.

We performed a similar comparison between our results based on different first-principles approaches. This is shown in Fig. 8, where the three curves follow a similar behavior. Notably, B3LYP, which is a hybrid DFT method involving both BLYP and HF contributions, leads to values that fall between the BLYP and RHF results.

As discussed earlier, since the VHS for zigzag nanotubes happen at the Γ point, we expect the spectra in Figs. 3 and 4 to be very close to the overall spectra of these nanotubes. A comparison with other first-principles calculations for the optical absorption spectra of an (8,0) nanotube in the 3–7 (Ref. 15) and 0–8 eV (Ref. 16) ranges confirms this point. The only peak missing in our calculation within this range is the one at around 4 eV that has been shown to occur at the X point of the band structure for a transition between the valence and conduction band with $m=\frac{n}{2}$. This is likely due to the high density of states for these bands at the X point of the band structure, which results in a non-negligible transition rate.

V. SUMMARY

In summary, the band-to-band transition dipole moment for (8,0), (10,0), and (7,0) zigzag nanotubes was calculated at the Γ point for 12 valence and 16 conduction bands in a wide range of wavelengths (infrared-visible-ultraviolet) using first-principles methods. We compared the results with the conventional selection rules for nanotubes. We noted that modified angular momentum numbers should be used in order to explain all the allowed transitions. We showed that

besides the π-π^* transitions, π-σ^*, σ-π^*, and σ-σ^* transitions also contribute to the optical spectrum. In fact, the dipole moment magnitude was shown to be highest for σ-σ^* transitions and some of these transitions resulted in a high probability of absorption in the low UV region. The trends in dipole moments, selection rules, and transition rates were similar in all the three nanotubes. We observed high transition rates in the infrared, visible and even low UV ranges. The maximum of absorption at the Γ point for (8,0), (10,0), and (7,0) nanotubes occurred at approximately 1.42 eV, 0.79 eV and 3.03 eV, respectively, and the strong peaks in the UV region were related to the σ-σ^* transitions in all the three nanotubes. By using first-principles approaches, the curvature effects were automatically taken into account. These effects could play an important role in the optical properties of nanotubes with small diameters.

ACKNOWLEDGMENTS

We thank Ian Affleck of the UBC Department of Physics and Astronomy for insightful discussions. This research has been enabled in part through the use of advanced computing resources provided by WestGrid and Compute/Calcul Canada. Financial support was provided by the Natural Sciences and Engineering Research Council (NSERC) under Grants No. 341629-07 and No. 43826-09, and SiliconPro.

*Corresponding author; anojeh@ece.ubc.ca

[1] M. O'Connell, S. Bachilo, C. Huffman, V. Moore, M. Strano, E. Haroz, K. Rialon, P. Boul, W. Noon, C. Kittrell, J. Ma, R. Hauge, R. Weisman, and R. E. Smalley, Science **297**, 593 (2002).

[2] S. Lebedkin, F. Hennrich, T. Skipa, and M. Kappes, J. Phys. Chem. B **107**, 1949 (2003).

[3] J. Lefebvre, J. M. Fraser, P. Finnie, and Y. Homma, Phys. Rev. B **69**, 075403 (2004).

[4] M. Freitag, Y. Martin, J. Misewich, R. Martel, and P. Avouris, Nano Lett. **3**, 1067 (2003).

[5] Y. Ohno, S. Kishimoto, T. Mizutani, T. Okazaki, and H. Shinohara, Appl. Phys. Lett. **84**, 1368 (2004).

[6] S. Bachilo, M. Strano, C. Kittrell, R. Hauge, R. E. Smalley, and R. Weisman, Science **298**, 2361 (2002).

[7] R. Weisman and S. Bachilo, Nano Lett. **3**, 1235 (2003).

[8] M. Sfeir, T. Beetz, F. Wang, L. Huang, X. Huang, M. Huang, J. Hone, S. O'Brien, J. Misewich, T. Heinz, L. Wu, Y. Zhu, and L. Brus, Science **312**, 554 (2006).

[9] G. Dukovic, F. Wang, D. Song, M. Sfeir, T. Heinz, and L. Brus, Nano Lett. **5**, 2314 (2005).

[10] S. Berciaud, L. Cognet, P. Poulin, R. B. Weisman, and B. Lounis, Nano Lett. **7**, 1203 (2007).

[11] C. D. Spataru, S. Ismail-Beigi, L. X. Benedict, and S. G. Louie, Phys. Rev. Lett. **92**, 077402 (2004).

[12] C. Spataru, S. Ismail-Beigi, L. X. Benedict, and S. Louie, Appl. Phys. A: Mater. Sci. Process. **78**, 1129 (2004).

[13] J. Neaton, K. Khoo, C. Spataru, and S. Louie, Comput. Phys. Commun. **169**, 1 (2005).

[14] A. Hagen and T. Hertel, Nano Lett. **3**, 383 (2003).

[15] Y. Takagi and S. Okada, Phys. Rev. B **79**, 233406 (2009).

[16] G. Luo, J. Zheng, J. Lu, W. N. Mei, L. Wang, L. Lai, J. Zhou, R. Qin, H. Li, and Z. Gao, J. Phys. Chem. C **113**, 10314 (2009).

[17] G. G. Samsonidze, R. Saito, N. Kobayashi, A. Grüneis, J. Jiang, A. Jorio, S. Chou, G. Dresselhaus, and M. S. Dresselhaus, Appl. Phys. Lett. **85**, 5703 (2004).

[18] R. Saito, A. Grüneis, G. G. Samsonidze, G. Dresselhaus, M. S. Dresselhaus, A. Jorio, L. Cancado, M. Pimenta, and A. G. Souza Filho, Appl. Phys. A: Mater. Sci. Process. **78**, 1099 (2004).

[19] J. Jiang, R. Saito, A. Grüneis, G. Dresselhaus, and M. S. Dresselhaus, Carbon **42**, 3169 (2004).

[20] E. Malić, M. Hirtschulz, F. Milde, A. Knorr, and S. Reich, Phys. Rev. B **74**, 195431 (2006).

[21] G. G. Samsonidze, A. Grüneis, R. Saito, A. Jorio, A. G. Souza Filho, G. Dresselhaus, and M. S. Dresselhaus, Phys. Rev. B **69**, 205402 (2004).

[22] A. Grüneis, R. Saito, G. G. Samsonidze, T. Kimura, M. A. Pimenta, A. Jorio, A. G. Souza Filho, G. Dresselhaus, and M. S. Dresselhaus, Phys. Rev. B **67**, 165402 (2003).

[23] X. Blase, L. X. Benedict, E. L. Shirley, and S. G. Louie, Phys. Rev. Lett. **72**, 1878 (1994).

[24] S. Reich, C. Thomsen, and P. Ordejon, Phys. Rev. B **65**, 155411 (2002).

[25] P. N. D'yachkov, H. Hermann, and D. Kirin, Appl. Phys. Lett. **81**, 5228 (2002).

[26] P. D'yachkov and H. Hermann, J. Appl. Phys. **95**, 399 (2004).

[27] H. Ajiki and T. Ando, Physica B **201**, 349 (1994).

[28] M. J. Frisch, G. W. Trucks, H. B. Schlegel, G. E. Scuseria, M. A. Robb, J. R. Cheeseman, J. A. Montgomery, Jr., T. Vreven, K. N. Kudin, J. C. Burant, J. M. Millam, S. S. Iyengar, J. Tomasi, V. Barone, B. Mennucci, M. Cossi, G. Scalmani, N. Rega, G. A. Petersson, H. Nakatsuji, M. Hada, M. Ehara, K. Toyota, R. Fukuda, J. Hasegawa, M. Ishida, T. Nakajima, Y. Honda, O. Kitao, H. Nakai, M. Klene, X. Li, J. E. Knox, H. P. Hratchian, J. B. Cross, V. Bakken, C. Adamo, J. Jaramillo, R. Gomperts, R. E. Stratmann, O. Yazyev, A. J. Austin, R. Cammi, C. Pomelli, J. W. Ochterski, P. Y. Ayala, K. Morokuma, G. A. Voth, P. Salvador, J. J. Dannenberg, V. G. Zakrzewski, S. Dapprich, A. D. Daniels, M. C. Strain, O. Farkas, D. K. Malick, A. D. Rabuck, K. Raghavachari, J. B. Foresman, J. V. Ortiz, Q. Cui, A. G. Baboul, S. Clifford, J. Cioslowski, B. B. Stefanov, G. Liu, A. Liashenko, P. Piskorz, I. Komaromi, R. L. Martin, D. J. Fox, T. Keith, M. A. Al-Laham, C. Y. Peng, A. Nanayakkara, M. Challacombe, P. M. W. Gill, B. Johnson, W. Chen, M. W. Wong, C. Gonzalez, and J. A. Pople, " GAUSSIAN 03, Revision C.02," Gaussian, Inc., Wallingford, CT, 2004.

[29] M. J. Frisch, G. W. Trucks, H. B. Schlegel, G. E. Scuseria, M. A. Robb, J. R. Cheeseman, G. Scalmani, V. Barone, B. Mennucci, G. A. Petersson, H. Nakatsuji, M. Caricato, X. Li, H. P. Hratchian, A. F. Izmaylov, J. Bloino, G. Zheng, J. L. Sonnenberg, M. Hada, M. Ehara, K. Toyota, R. Fukuda, J. Hasegawa, M. Ishida, T. Nakajima, Y. Honda, O. Kitao, H. Nakai, T. Vreven, J. A. Montgomery, Jr., J. E. Peralta, F. Ogliaro, M. Bearpark, J. J. Heyd, E. Brothers, K. N. Kudin, V. N. Staroverov, R. Koba-

yashi, J. Normand, K. Raghavachari, A. Rendell, J. C. Burant, S. S. Iyengar, J. Tomasi, M. Cossi, N. Rega, J. M. Millam, M. Klene, J. E. Knox, J. B. Cross, V. Bakken, C. Adamo, J. Jaramillo, R. Gomperts, R. E. Stratmann, O. Yazyev, A. J. Austin, R. Cammi, C. Pomelli, J. W. Ochterski, R. L. Martin, K. Morokuma, V. G. Zakrzewski, G. A. Voth, P. Salvador, J. J. Dannenberg, S. Dapprich, A. D. Daniels. Farkas, J. B. Foresman, J. V. Ortiz, J. Cioslowski, and D. J. Fox, " GAUSSIAN 09, Revision A.1," Gaussian Inc. Wallingford CT, 2009.

[30] A. D. Becke, Phys. Rev. A **38**, 3098 (1988).

[31] C. Lee, W. Yang, and R. G. Parr, Phys. Rev. B **37**, 785 (1988).

[32] P. Stephens, F. Devlin, C. Chabalowski, and M. Frisch, J. Phys. Chem. **98**, 11623 (1994).

[33] M. Damnjanović, I. Milošević, T. Vuković, and J. Maultzsch, J. Phys. A: Math. Gen. **36**, 5707 (2003).

[34] S. Reich, J. Maultzsch, C. Thomsen, and P. Ordejon, Phys. Rev. B **66**, 035412 (2002).

[35] T. Saito, S. Ohshima, T. Okazaki, S. Ohmori, M. Yumura, and S. Iijima, J. Nanosci. Nanotechnol. **8**, 6153 (2008).

[36] T. Pichler, M. Knupfer, M. S. Golden, J. Fink, A. Rinzler, and R. E. Smalley, Phys. Rev. Lett. **80**, 4729 (1998).

[37] S. Datta, *Quantum Transport: Atom to Transistor* (Cambridge University Press, Cambridge, 2005).